Polymer-Coated Gold Nanoparticles

Fabrication of Ordered Arrays of Gold Nanoparticles Coated with High-Density Polymer Brushes**

*Kohji Ohno, Kyoungmoo Koh, Yoshinobu Tsujii, and Takeshi Fukuda**

The synthesis and characterization techniques of monodisperse nanoparticles have rapidly developed, thus stressing the importance of organizing those particles into an ordered assembly to obtain new properties, which may arise from their collective interactions in the ordered state.[1,2] Sun et al. reported that controlled evaporation of solvent with nanoparticles dispersed in it, followed by thermal treatment led to a self-organized, close-packed assembly of the particles.[3,4] Several groups created ordered arrays of nanoparticles by using the Langmuir-Blodgett (LB) technique[5,6] or the self-organization of block copolymers.[7] These studies, however, only provided ordered arrays of nanoparticles with a limited area and controllability of interparticle distance.

We recently applied the surface-initiated living radical-polymerization (LRP) technique[8–14] to form polymer brushes on Au-nanoparticle surfaces with a controlled chain length and chain-length distribution, and a graft density as high as 0.3 chains nm^{-2}.[15] In a solvent-cast film of the Au-nanoparticle–polymer hybrid as observed by transmission electron microscope (TEM), the metal cores of the hybrid particles were uniformly dispersed in the matrix of the brush polymer without forming any aggregates. However, this Au-nanoparticle assembly was poorly ordered, mainly because of the broad size distribution of the Au nanoparticles (relative standard deviation $\sigma = 49.7\,\%$). In this work, we have attempted to broaden the science and technology of the Au nanoparticle coated with a high-density polymer brush, with the aim of fabricating ordered and controllable assemblies of metal particles.

A narrowly size-distributed Au nanoparticle with LRP-initiating groups was synthesized by a simple one-pot reaction as follows: An aqueous solution of citric acid trisodium salt (140 mM, 20 mL) was quickly added to vigorously stirring boiling water (1.5 L) containing tetrachloroaurate (230 mg). After 5 min, the reaction was cooled in an ice bath for 10 min. To this mixture the initiator 11,11′-dithiobis[1-(2-bromo-2-methylpropionyloxy)undecane][10] (70 mg) dissolved in THF (500 mL) was added, and this mixture was stirred for another 12 h. The resulting crude Au nanoparticles were purified by using a reported method.[15] TEM revealed that the average

[*] Prof. Dr. T. Fukuda, Dr. K. Ohno, K. Koh, Dr. Y. Tsujii
Institute for Chemical Research, Kyoto University
Uji, Kyoto 611-0011 (Japan)
Fax: (+81) 774-38-3170
E-mail: fukuda@scl.kyoto-u.ac.jp

[**] This work was supported in part by a Grant-in-Aid for Scientific Research (Grant-in-Aid 14205131, 14750695) from the Ministry of Education, Culture, Sports, Science and Technology, Japan.

 DOI: 10.1002/ange.200250850

diameter of the purified particles was about 12 nm, with a fairly narrow size distribution ($\sigma = 11.4\,\%$).

The copper-mediated LRP[16] of methyl methacrylate (MMA) was carried out with the initiator-coated Au nanoparticles by using a reported method.[15] The resultant Au-nanoparticle–poly(methyl methacrylate) (PMMA) hybrids were purified repeatedly by a fractional reprecipitation technique, and it was confirmed by gel permeation chromatography (GPC) that the thus purified Au-nanoparticle–PMMA hybrids contained no free polymers.[15] The $\bar{M}_n$ values of the PMMAs cleaved from the Au-nanoparticle surface were 12000, 28000, and 62000, and their polydispersity indexes $\bar{M}_w/\bar{M}_n$ were 1.23, 1.33, and 1.49, respectively, according to GPC. The graft density was estimated to be about 0.4 chains nm^{-2} for each of the three samples. This figure means that an Au nanoparticle has on average 180 PMMA grafts on its surface.

Each of the Au-nanoparticle–PMMA hybrids thus prepared was dissolved in benzene at a concentration about 1 mg mL^{-1}. The solution was deposited onto the surface of purified water in a circular Langmuir trough equipped with a circular compression barrier.[17] The surface film was compressed at a constant speed of 60 mm^2 min^{-1} by the circular barrier. The surface pressure π was measured by a filter paper Wilhelmy plate. A typical isotherm of the surface pressure, π, versus occupied area, A, is given in Figure 1. In this example, π deviates from zero at a critical surface pressure, A_{crit}, of 13600 nm^2 per particle. With a further compression, π increases gradually at first, and passing through a shoulder at around $A = 8000$, it increases steeply for A smaller than about 5000 nm^2 per particle. The other Au-nanoparticle–PMMA hybrids showed qualitatively a similar behavior.

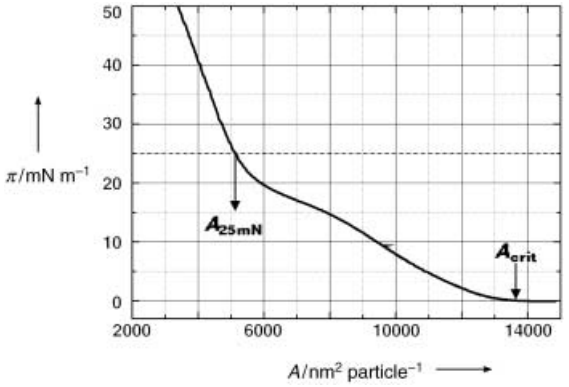

Figure 1. Isotherm of the surface pressure, π, versus occupied area A for the surface film of Au-nanoparticle–PMMA hybrid. $\bar{M}_n$ of the graft polymer is 28000.

All the surface films of Au-nanoparticle–PMMA hybrids were successfully transferred onto a carbon-coated copper TEM grid mounted on a glass plate (sputtered with reduced-pressure air just before use) by the LB deposition (vertical lifting-up) technique at a constant π of 25 mN m^{-1} and a constant speed of 1 mm min^{-1}. Figures 2a–d shows the TEM images of the transferred films. For comparison, the TEM image of the initiator-coated Au-nanoparticle monolayer is

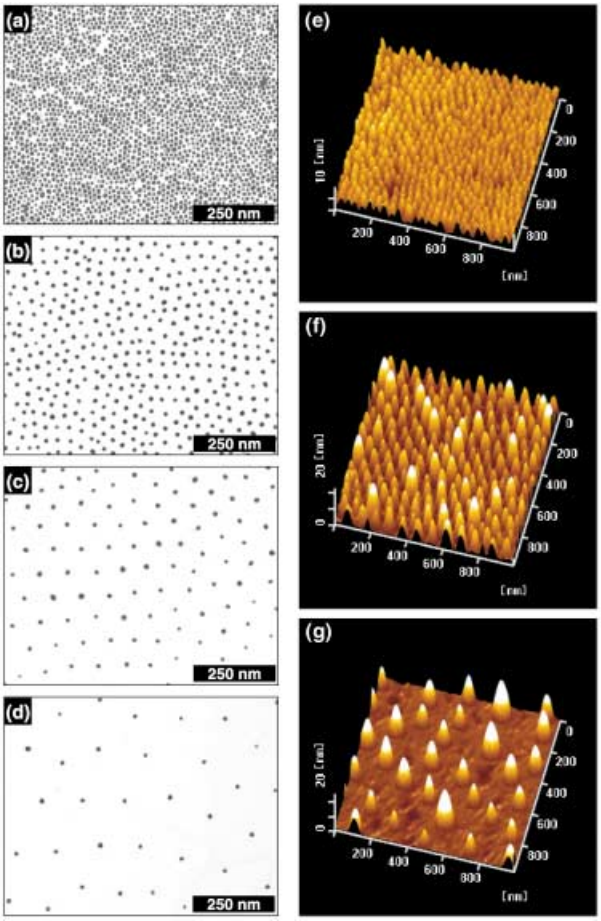

Figure 2. TEM micrographs of the transferred films of (a) initiator-coated Au nanoparticles and (b–d) Au-nanoparticle–PMMA hybrids: $\bar{M}_n$ of the PMMA graft = (b) 12000, (c) 28000, and (d) 62000. (e–g) AFM images of the transferred films of Au-nanoparticle–PMMA hybrids: $\bar{M}_n$ of the PMMA graft = (e) 12000, (f) 28000, and (g) 62000.

also shown (Figure 2a), which was prepared under exactly the same conditions as for the Au-nanoparticle–PMMA films, except that a mixture of THF/chloroform (1:1 by volume) was used as the solvent. The TEM images show that the Au-nanoparticle cores visible as dark circles are uniformly dispersed throughout the film, while the PMMA chains, which should be forming fringes surrounding the Au-nanoparticle cores, are invisible because of their much lower electron density. Noteworthy are the high degree of positional order of the Au-nanoparticle cores present in the hybrid films and the strong dependence of the interparticle distance on the chain length of PMMA grafts. Questions now arise as to the detailed structure of the monolayer film, of the individual hybrid particles, and the conformation of the individual PMMA grafts on the substrate and hence at the air–water surface.

To shed light on these questions, we have observed the same monolayer films transferred onto a freshly cleaved mica substrate (at $\pi = 25$ mN m^{-1}) on an atomic force microscope (AFM, Seiko Instruments Inc., SPA-400). The AFM images given in Figure 2e–g exhibit protrusions whose height and thickness both increase with increasing chain length of

PMMA grafts. In the AFM image in Figure 2g, for example, the protrusions are standing on the rather flat but rough surface, which is not the substrate (mica) surface but a PMMA matrix, as a mica surface should look perfectly smooth at this magnification. The mean height of the protrusions measured from the lowest surface of the matrix is about 20 nm, which roughly compares to the size of the "compact core–shell model" consisting of the Au-nanoparticle core and the PMMA shell of the bulk density (Figure 3a). These observations suggest the structural model of the hybrid film as is schematically illustrated in Figure 3c.

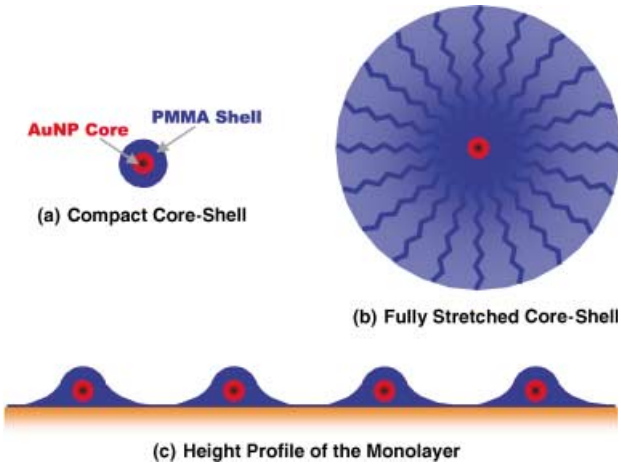

Figure 3. Schematic representations of (a) the compact core-shell model, (b) the fully stretched core-shell model, and (c) the height profile of the Au-nanoparticle–PMMA ($\bar{M}_n = 28000$) hybrid monolayer on the substrate surface transferred at 25 mN m^{-1}.

Figure 4 shows the mean nearest-neighbor center-to-center distance D of the Au-nanoparticle–PMMA hybrid at $\pi = 25$ mN m^{-1} (D_{25mN}) as a function of the PMMA graft molecular weight. Figure 4 also shows the D value at $A = A_{crit}$ calculated with $D_{crit} = D_{25mN}(A_{crit}/A_{25mN})^{1/2}$, where A_{crit} and A_{25mN} are the values of A read from the π–A isotherm (cf. Figure 1). The diameters of the compact core–shell model and the "fully stretched core–shell model" are also shown. (The diameter is equal to D for the 2D hexagonal close packing of spherical models.) The latter model consists of the Au-nanoparticle core and the PMMA shell whose size is equal to that of the PMMA chains radially stretched in all *trans* conformation (Figure 3b). Figure 4 shows that D_{25mN} is much larger than the diameter of the compact core–shell model. It is as large as about half that of the fully stretched core–shell model. This means that the PMMA shell is not compact but has an extremely large extension in the film-surface direction, thus producing the strong hindrance against compression. This picture is consistent with the AFM observation presented above. According to Rondelez et al.,[18] PMMA at the air–water interface has a slightly negative second virial coefficient and the radius of gyration R_G proportional to $M^{0.57}$. This factor means that even though water does not dissolve PMMA, it swells PMMA and allows it to have a random coil conformation at the air–water interface. If, then,

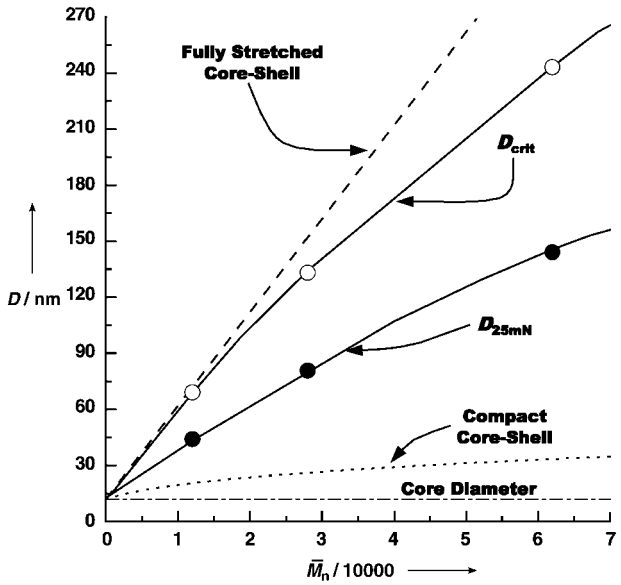

Figure 4. Plot of the mean nearest-neighbor center-to-center distance D as a function of $\bar{M}_n$ of the PMMA graft. The broken and dotted lines represent the diameters of the fully stretched and compact core–shell models, respectively.

we assume that the PMMA chains on the Au-nanoparticle surface have the random coil conformation suggested above, we estimate the size of the PMMA shell to be about the same as that of the compact core–shell model (the thickness of the "compact" shell is already quite large because of the high graft density). Even more surprising is the magnitude of D_{crit}. This parameter will characterize the critical surface concentration[18] at which the PMMA fringes from different particles begin to overlap with each other. Figure 4 shows that D_{crit} is nearly as large as the diameter of the fully stretched core–shell model. This strongly suggests that the fringe PMMA chains are nearly fully stretched at the air–water interface.

We reported that the PMMA brush formed on a silicon wafer with a similarly high surface density[8] and swollen by toluene had an equilibrium film thickness as much as 80 to 90% of the end-to-end distance of the fully stretched PMMA chain.[19,20] Namely the PMMA chains in this high-density brush were almost fully extended. This phenomenon was interpreted as being a consequence of the strong anisotropic interactions among polymer chains arising from the high surface density. The observations described above show that a similar phenomenon does occur in a 2D system like the air–water interface. Aside from the difference in dimensionality, the surface on which the brush is formed is spherical in the work reported herein, not flat like the silicon wafer used in previous work.[19,20] Accordingly, the polymer density decreases with increasing distance from the core center. For a fixed core diameter, the anisotropic interaction that causes the chain extension will, therefore, become weaker as the chain length of the brush increases. This effect manifests itself in the downward curvature observed for both the D_{crit} and D_{25mN} versus $\bar{M}_n$ plot in Figure 4.

In conclusion, we have synthesized a narrowly size-distributed Au nanoparticle coated with a well-defined,

high-density PMMA. Because of the high surface density and the controlled chain length, the PMMA grafts at the air–water interface exert interparticle interactions of an extremely long range, a range comparable to the full length of the PMMA chain. Consequently, the Au nanoparticles form a 2D array with a high degree of structural order and exceptionally wide controllability of the interparticle distance. Owing to the simplicity and versatility of surface-initiated LRP, this work may be extended to other metal and semiconductor nanoparticles for their 2D or 3D ordered assemblies with wide controllability of lattice parameters. The degree of structural order attainable by this strategy depends primarily on the size uniformity of the nanoparticles.

Received: December 27, 2002
Revised: February 20, 2003 [Z50850]

Keywords: gold · nanostructures · nanotechnology · ordered arrays · polymers

[1] D. L. Feldheim, C. D. Keating, *Chem. Soc. Rev.* **1998**, *27*, 1.
[2] C. P. Collier, T. Vossmeyer, J. R. Heath, *Annu. Rev. Phys. Chem.* **1998**, *49*, 371.
[3] S. Sun, C. B. Murray, D. Weller, L. Folks, A. Moser, *Science* **2000**, *287*, 1989.
[4] S. Sun, H. Zeng, *J. Am. Chem. Soc.* **2002**, *124*, 8204.
[5] J. R. Heath, C. M. Knobler, D. V. Leff, *J. Phys. Chem. B* **1997**, *101*, 189.
[6] J. J. Brown, J. A. Porter, C. P. Daghlian, U. J. Gibson, *Langmuir* **2001**, *17*, 7966.
[7] J. P. Spatz, S. Mössmer, C. Hartmann, M. Möller, T. Herzog, M. Krieger, H.-G. Boyen, P. Ziemann, B. Kabius, *Langmuir* **2000**, *16*, 407.
[8] M. Ejaz, S. Yamamoto, K. Ohno, Y. Tsujii, T. Fukuda, *Macromolecules* **1998**, *31*, 5934.
[9] T. von Werne, T. E. Patten, *J. Am. Chem. Soc.* **2001**, *123*, 7494.
[10] R. R. Shah, D. Merreceyes, M. Husemann, I. Rees, N. L. Abbott, C. J. Hawker, J. L. Hedrick, *Macromolecules* **2000**, *33*, 597.
[11] J. Pyun, K. Matyjaszewski, T. Kowalewski, D. Savin, G. Patterson, G. Kickelbick, N. Huesing, *J. Am. Chem. Soc.* **2001**, *123*, 9445.
[12] J.-B. Kim, M. L. Bruening, G. L. Baker, *J. Am. Chem. Soc.* **2000**, *122*, 7616.
[13] H. Mori, A. Boker, G. Krausch, A. H. E. Müller, *Macromolecules* **2001**, *34*, 6871.
[14] R. A. Sedjo, B. K. Mirous, W. J. Brittain, *Macromolecules* **2000**, *33*, 1492.
[15] K. Ohno, K. Koh, Y. Tsujii, T. Fukuda, *Macromolecules* **2002**, *35*, 8989.
[16] T. E. Patten, J. Xia, T. Abernathy, K. Matyjaszewski, *Science* **1996**, *272*, 866.
[17] M. Matsumoto, Y. Tsujii, K. Nakamura, T. Toshimoto, *Thin Solid Films* **1996**, *280*, 238.
[18] D. Poupinet, R. Vilanove, F. Rondelez, *Macromolecules* **1989**, *22*, 2491.
[19] S. Yamamoto, M. Ejaz, Y. Tsujii, M. Matsumoto, T. Fukuda, *Macromolecules* **2000**, *33*, 5602.
[20] S. Yamamoto, M. Ejaz, Y. Tsujii, T. Fukuda, *Macromolecules* **2000**, *33*, 5608.

